Erschienen in: Solar Energy Materials and Solar Cells. Elsevier. 2022, 246, 111890
https://doi.org/10.1016/j.solmat.2022.111890

Poly-Si thickness and temperature dependent oxide disruption induced by penetration of the interfacial oxide in (p) poly-Si/SiO_x passivating contacts

Jonathan Linke [a,1,*], Raphael Glatthaar [a,1], Frank Huster [a], Tobias Okker [a], Sören Möller [b], Giso Hahn [a], Barbara Terheiden [a]

[a] *University of Konstanz, D-78457, Konstanz, Germany*
[b] *Forschungszentrum Jülich GmbH, Institute of Energy and Climate Research, D-52425, Jülich, Germany*

ARTICLE INFO

Keywords:
Poly-Si
Interfacial oxide
Boron diffusion
Oxide disruption
Passivating contact
Sputtering

ABSTRACT

Passivating contacts based on polycrystalline silicon on an interfacial oxide (poly-Si/SiO_x) require a fine-tuned in-diffused dopant profile at the surface of the crystalline silicon wafer. In particular, a strong dopant in-diffusion causes excessive recombination. This study contributes to reveal the yet unclear mechanism of this degradation of passivation. Boron in-diffusion from co-sputtered (p) poly-Si layers through the interfacial oxide is investigated for several layer thicknesses and plateau temperatures during the solid phase crystallization. It is shown that for higher temperatures and unexpectedly also for thicker layers the observed recombination current density increases up to a total loss of passivation, accompanied by a physical interfacial oxide disruption, which is not observed for intrinsic reference layers. This behavior is supported by simple numerical calculations. The recombination current densities are transferred into the actual surface recombination velocity which in turn reveals an exponential increase towards higher boron concentrations at the interface between the oxide and the crystalline Si base. It is concluded that rather dopant penetration of the interfacial oxide is responsible for the degradation of passivation than the actual boron concentration at the interface itself as reported before in literature.

1. Introduction

In recent years, passivating contacts based on highly doped polycrystalline silicon (poly-Si) on top of an interfacial oxide (poly-Si/SiO_x) have been studied extensively [1–3] and are seen as key technology for future photovoltaic applications [4]. Most commonly, the fabrication process of such passivating contacts involves a high temperature anneal above 800°C for several minutes in order to crystallize previously deposited amorphous silicon (a-Si) to poly-Si and simultaneously to diffuse dopants from the poly-Si through the interfacial oxide into the crystalline silicon (c-Si) base. In this way, a shallow dopant tail is formed below the interfacial oxide which enhances carrier selectivity [5,6].

In the context of bipolar junction transistors, which utilized highly doped poly-Si as the emitter [7], as well as for state-of-the-art high-efficiency solar cells it was repeatedly reported, that the penetration of dopants through the interfacial oxide into the c-Si base dramatically influences the performance of the device [6,8]. In particular, starting from zero dopant in-diffusion, a stronger in-diffusion in terms of peak concentration and/or depth of the shallow dopant tail reduces the recombination at the poly-Si/SiO_x contact down to a minimum due to enhanced shielding of minority carriers. However, for even stronger in-diffusion the recombination increases again. This effect was observed for both polarities, i.e. boron [9], phosphorus [5,9] and arsenic [10]. As the diffusivity of phosphorus in the interfacial oxide is quite low compared to boron and arsenic [11], it is easier to control the in-diffusion of phosphorus, which seems to be one of the reasons for the present superiority of phosphorus doped (n) poly-Si/SiO_x contacts [1].

Even though the increase in recombination in the poly-Si/SiO_x structure for strong in-diffusion is well-known, a detailed microscopic explanation is still lacking. Auger recombination in the in-diffused shallow dopant tail was shown to play a minor role [12]. It was proposed that the penetration of dopants induces defects in the interfacial oxide and thus increases the surface recombination velocity [5]. At least for boron penetration a degradation mechanism via a reaction of oxide

* Corresponding author. Now with ISC Konstanz e.V., D-78467 Konstanz, Germany.
E-mail address: jonathan.linke@uni-konstanz.de (J. Linke).
[1] Authors contributed equally.

defects with holes was suggested in the context of the negative bias temperature instability, which induces a negative threshold voltage shift in (p) poly-Si gate MOSFETs [13]. As pinhole formation in the interfacial oxide during the high temperature anneal was found to play a critical role for majority carrier transport [14], these pinholes might also contribute to this increase in recombination in the poly-Si/SiO_x structure, depending on the individual pinhole density [8]. In this context, pinholes were shown to grow with both temperature and duration up to the extreme case of the formation of oxide "balls" (balling-up) with a minimum radius of three times the original oxide thickness separated by large regions of un-passivated poly-Si/c-Si interfaces [15,16].

This study contributes to reveal the mechanism behind the increase in recombination in the poly-Si/SiO_x structure for strong dopant in-diffusion by a variation of the poly-Si layer thickness. Most investigations regarding the poly-Si thickness relied on ex-situ doping [5,17,18] as the hydrogen-induced blistering issue of chemical vapor deposited (CVD) a-Si:H layers often limits the layer thickness to <50 nm [6,19–21], which is especially a problem for boron doped layers. In this study, an initially amorphous (p) a-Si layer was deposited by in-situ boron doped magnetron co-sputtering whose suitability for poly-Si/SiO_x contacts was previously demonstrated [22]. These sputtered a-Si layers are basically hydrogen-free so that blistering issues during the high temperature anneal are completely avoided, enabling to investigate a wider range of poly-Si layer thicknesses. Keeping the boron concentration constant, the poly-Si thickness was varied between 27 and 117 nm and different levels of dopant in-diffusion were achieved by varying the high temperature anneal between 890 and 950°C. It is known that the temperature variation provides rather coarse changes of the in-diffused shallow dopant tail, while the thickness variation is expected to cause small-scale changes as only the absolute number of boron atoms available for diffusion is increased.

2. Materials and methods

2.1. Sample preparation

Symmetrical (p) poly-Si/SiO_x/c-Si test samples were processed on Czochralski-grown silicon (Cz) wafers (n-type, ~35 Ωcm, 5x5 cm^2, ~150 µm). After a saw damage etch and piranha clean of the Cz substrates, an interfacial thermal oxide was grown at a temperature of 625°C, resulting in a thickness of ~1.7 nm as determined by spectroscopic ellipsometry. Subsequently, in-situ doped (p) a-Si layers were deposited by magnetron co-sputtering (AJA ATC 2200, AJA International Inc.) using a pure silicon target (6 N, 3.7 W/cm^2) and a pure boron target (3 N, 1.8 W/cm^2) in Ar ambient at 2 mTorr and a table heater set temperature of 450°C. Solely the process duration was adjusted between 750 and 3000 s to achieve different mean poly-Si layer thicknesses of 27–117 nm as determined by spectroscopic ellipsometry following the procedure described in Ref. [21]. Immediately after a wet chemical ozone-cleaning, the samples were subjected to a high temperature anneal in a conventional tube furnace with plateau temperatures of 890/920/950°C in N_2 ambient. The set load/unload temperature (780°C), heating/cooling rates as well as the total process duration (90 min) were kept constant resulting in different plateau durations of 41.25 min/30 min/18.75 min. In this way, it is ensured that the duration of exposure to temperatures equal to or above 890°C is the same for all three processes, thus providing a higher degree of comparability with respect to boron diffusion.

Reference samples with intrinsic (i) poly-Si layers were processed equally except of using only the silicon target for a-Si deposition. In this way, the total deposition rate during sputtering is reduced, which was compensated by slightly increased process durations in order to yield layer thicknesses comparable to the doped (p) poly-Si layers.

For hydrogenation of the symmetrical test samples with the doped layers, a hydrogen-rich silicon nitride (SiN_x) was plasma-enhanced chemical vapor deposited (PECVD, Plasmalab System 100, Oxford Instruments) on top of the (p) poly-Si layer and subsequently the samples were fired at a set peak temperature of 819°C in a conventional fast firing belt furnace. For subsequent pinhole magnification as described in Ref. [23], the SiN_x layer was removed in 10% hydrofluoric acid and the underlying (p) poly-Si layer was exposed to 30% TMAH.

2.2. Characterization

The characterization of the samples was done at several stages during the process as depicted in Fig. 1. The recombination current density at the contact J_0 was measured by photoconductance decay measurements (PCD, Sinton lifetime tester WCT120, Sinton Instruments Inc.) corrected as described in Ref. [24]. A relative uncertainty of 8% was assumed [25]. Electrochemical capacitance-voltage profiling (ECV, Wafer Profiler CVP21, WEP) was used to measure quantitatively the active boron (hole) concentration profiles $n_h(z)$ as a function of the depth z, while glow discharge optical emission spectroscopy (GD-OES, GDA 750 HR, Spectruma Analytik GmbH) as well as secondary ion mass spectroscopy[2] (SIMS) were used to measure qualitatively the chemical boron concentration $n_B(t)$ as a function of the sputter time t in both the (p) poly-Si layer as well as in the substrate. GD-OES was also utilized to gain information about the interfacial oxide from the corresponding oxygen signal. After TMAH etch based pinhole magnification, regions of 506 μm^2 were recorded using scanning electron microscopy (SEM) in order to count the evolved etch pits. The resulting etch pit density (EPD) was interpreted as the original pinhole density n_{pin} in the interfacial oxide.

2.3. Simulation

Furthermore, FlexPDE [26] was used to numerically solve the 1D diffusion equation for the (p) poly-Si/SiO_x/c-Si structure according to Fick's law. The (p) poly-Si and interfacial oxide thicknesses were set to the values determined by spectroscopic ellipsometry (27–117 nm and 1.7 nm, respectively), while the thickness of the c-Si region followed from the boundary condition of a fixed thickness of 300 nm for the whole structure. The diffusivities in the (p) poly-Si, interfacial oxide and

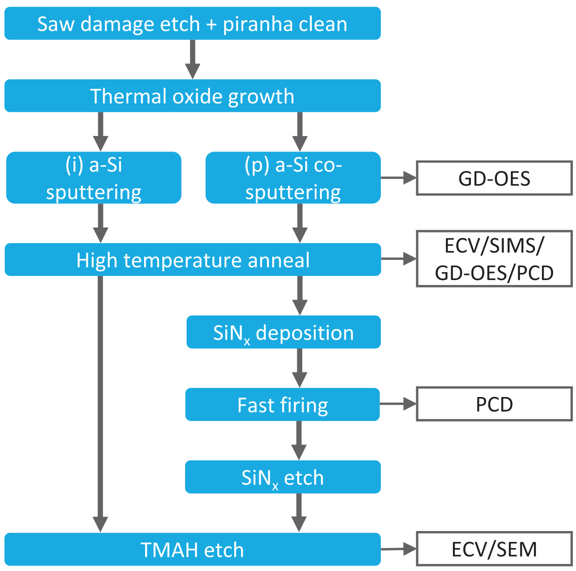

Fig. 1. Process flow of samples with both doped and intrinsic poly-Si layers as well as applied characterization methods at several stages of the process.

[2] SIMS measurements conducted at Forschungszentrum Jülich GmbH, Institute of Energy and Climate Research.

c-Si base were taken from Ref. [8]. The thermal dependencies of the diffusivities were considered using the set temperature profiles as a function of the process time of the different high temperature anneals as described above.

3. Results and discussion

3.1. Passivation

Fig. 2 presents the passivation quality in terms of recombination current density J_0 before (a) and after (b) hydrogenation, while the overall trends are the same and therefore discussed simultaneously. For the thin poly-Si layers (~27 nm) values slightly above 10 fA/cm^2 were measured after hydrogenation regardless of the annealing temperature. In contrast, for increasing layer thicknesses up to ~117 nm a clear temperature dependence was found: At 890°C the passivation quality is independent of the layer thickness, while at 920°C the recombination current density is strongly increased for >57 nm and at 950°C this increase occurs already for >27 nm thick layers and is even stronger up to ~630 fA/cm^2 after hydrogenation. The temperature dependence was partly expected in the context of a stronger dopant in-diffusion through the interfacial oxide. However, the strong loss in passivation quality for thicker layers in the absence of blistering is surprising and cannot be explained by the temperature alone.

A correlation of these strong increases in recombination can be found in the corresponding ECV and SIMS depth profiles as depicted in Fig. 3. First of all, the SIMS profiles confirm an identical and homogeneously distributed total boron concentration in the poly-Si layers regardless of the actual layer thickness. At 890°C annealing temperature all profiles show a shallow dopant tail and no significant differences for all poly-Si layer thicknesses in both the ECV and SIMS profiles. This observation corresponds to the constant low recombination current density in Fig. 2. At 920°C a deeper in-diffusion is visible for thicker poly-Si layers, with a pronounced higher interface concentration for the sample with ~117 nm thick layer. A similar behavior was also found for 950°C, while the disproportionately strong in-diffusion and high interface concentration is already observable at ≥57 nm layer thickness. Both strong in-diffusions at 920°C and 950°C correspond to significantly larger recombination current densities as shown in Fig. 2 (open symbols). Hence, a strong boron in-diffusion and high boron interface concentration can safely be linked to strong recombination. From the perspective of the temperature variation, this conclusion is well-known and not surprising. But from the perspective of the layer thickness variation in face of equal boron concentration in the poly-Si layer, such huge differences in boron in-diffusion and in absence of blistering are quite unexpected.

3.2. Interfacial oxide disruption as origin of the poly-Si thickness dependency

In order to investigate this unexpected layer thickness dependency in more detail, FlexPDE was utilized to solve Fick's diffusion law in 1D with the ECV determined active boron concentration of the (p) poly-Si layers as input. Fig. 4 exemplarily shows the resulting boron depth profiles of all layer thicknesses for a high temperature anneal at 950°C. Thicker layers show a slightly stronger in-diffusion and a larger boron concentration at the interface as well as within the poly-Si layer, while all these concentrations are lower than the initial concentrations (horizontal dashed line). These observations are intuitively explained by the larger absolute number of boron atoms present in the poly-Si layer for thicker layers, hence larger diffusion reservoir. However, with respect to the huge in-diffusion differences observable in the ECV and SIMS profiles (Fig. 3), this simulated effect seems to be rather weak and cannot be the only explanation for these measured profiles.

In fact, utilizing EDNA [27] to determine the Auger recombination within the in-diffused part of the ECV profiles of the samples with high recombination and strong boron in-diffusion leads to values in the range of 5–16 fA/cm^2. Compared to the measured values of up to ~630 fA/cm^2, it is evident that Auger recombination cannot explain these values and thus another predominant mechanism has to be identified.

A hint for such a mechanism is provided by the observation, that at 950°C the ECV profiles are basically identical for all poly-Si layer thicknesses between 57 and 117 nm, except for the deepest few nm (Fig. 3 c,f). Two possible explanations are suggested: First, the chemical boron concentration has reached the solid state solubility limit in silicon of ~10^{20} cm^{-3} at 950°C [28], which is compatible with the boron concentration at the interface determined by ECV (Fig. 3c). Or second, a structure similar to a boron-rich layer has evolved as known from borosilicate-glass based diffusion processes [29,30]. In both cases, it can be assumed that the interfacial oxide is consumed or disrupted. Clearly, this hypothesis would also explain the simultaneous strong increase in recombination as the chemical passivation ability of the interfacial oxide would be equally destroyed (open symbols in Fig. 2).

A strong indication for the validity of the hypothesis of disrupted interfacial oxides was found during the TMAH etch process originally meant for pinhole magnification. This etch process is expected to stop at the interfacial oxide, which was not the case for some samples. Table 1 indicates for which samples the etch process did not stop at the interface (values marked by round brackets) and shows the corresponding recombination current densities (same values as in Fig. 2). Clearly, no TMAH etch stop correlates with significantly larger recombination. This correlation holds not only for higher annealing temperatures, where a physical disruption was reported before in literature [15,16], but

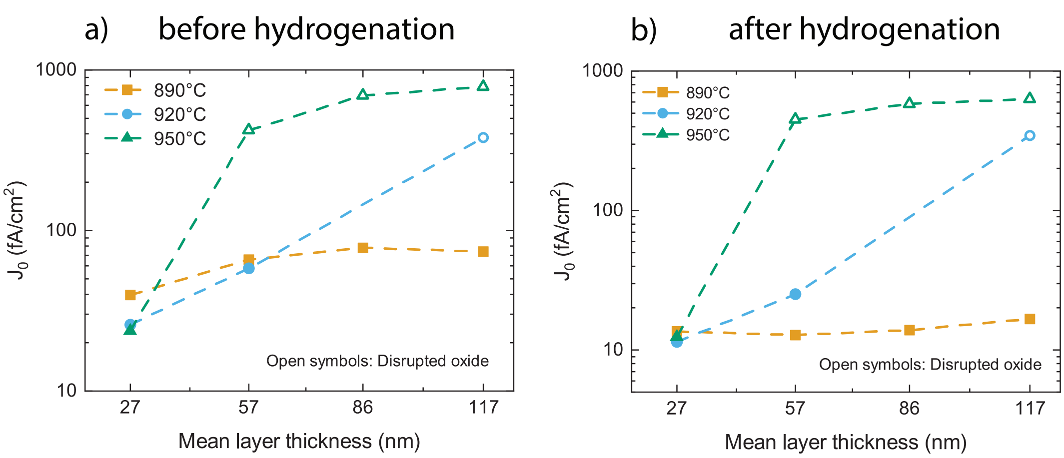

Fig. 2. PCD measured recombination current density J_0 a) before and b) after hydrogenation as a function of the mean poly-Si layer thickness and for all three annealing temperatures. Open symbols correspond to samples with disrupted interfacial oxide.

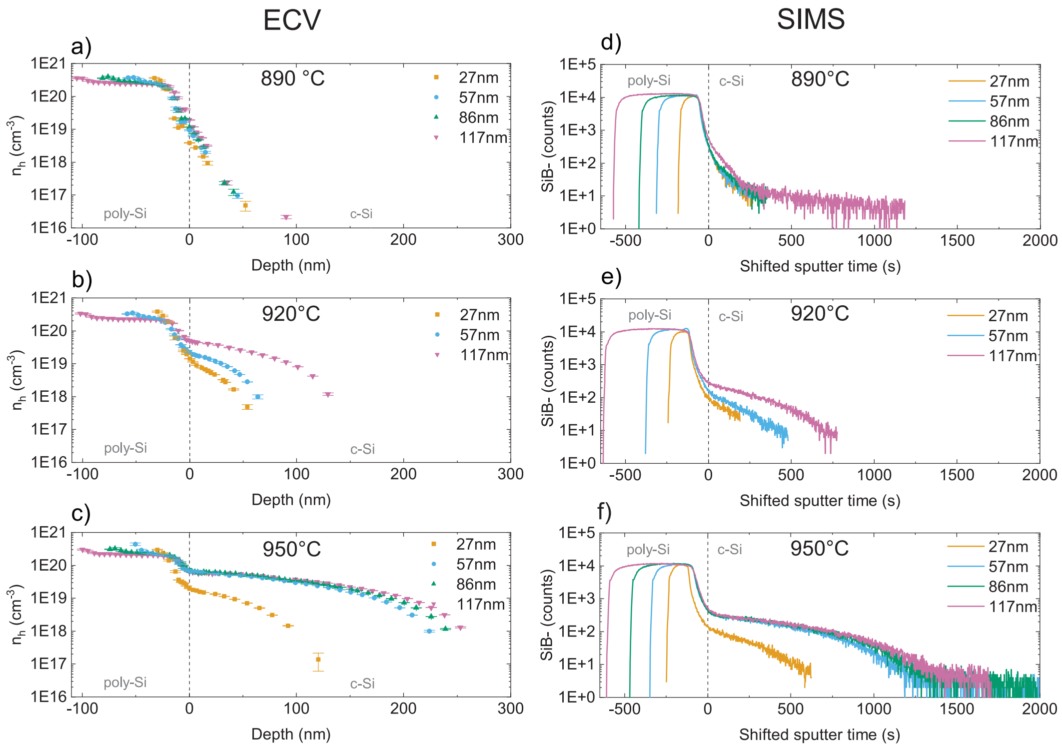

Fig. 3. a,b,c) ECV measured depth profiles of the active boron and d,e,f) SIMS measured depth profiles of the SiB-channel as measure for the chemical boron concentration of samples after the high temperature anneals sorted by temperature. The vertical dashed line is the approximated location of the interfacial oxide with poly-Si on the left and the c-Si base on the right side.

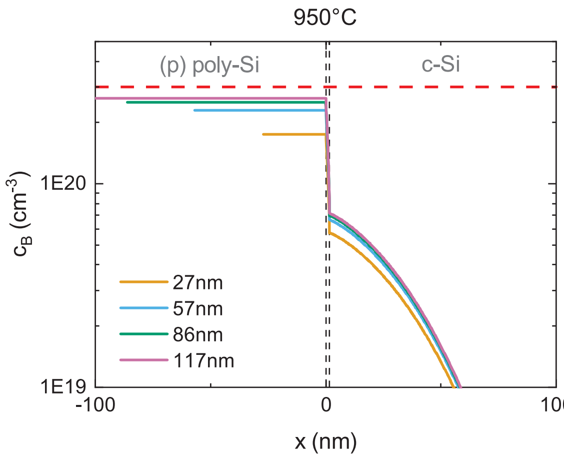

Fig. 4. Boron depth profiles as simulated by FlexPDE. The vertical dashed lines mark the region of the interfacial oxide (1.7 nm thickness) with poly-Si on the left and the c-Si base on the right side. The horizontal dashed line indicates the initial boron concentration used as input for the simulation.

Table 1
Samples for which the TMAH etch process did not stop, marked by round brackets around the PCD measured recombination current densities after hydrogenation (same values as in Fig. 2).

	J_0 (fA/cm^2)	(p) poly-Si thickness			
		26 nm	57 nm	86 nm	117 nm
Annealing temperature	**890°C**	14	13	14	17
	920°C	11	25	–	(344)
	950°C	12	(449)	(581)	(631)

notably also for increasing poly-Si layers thickness.

The hypothesis of an underlying interfacial oxide disruption is further supported by the SEM images in Fig. 5. Large scale inverted pyramid frustums with a size of a few µm as typical for global TMAH etching of the silicon base were found throughout all samples without etch stop (Fig. 5a). In contrast, small scale inverted pyramids ~100 nm can be seen as locally under-etched interfacial oxide and thus magnified pinholes on samples with global etch stop (Fig. 5b).

Yet another indication of the presence of interfacial oxide disruptions is the depth resolved oxygen signal measured by GD-OES and corrected according to Ref. [31]. The interfacial oxide appears as a peak in the raw depth profile as exemplarily shown in Fig. 6a for the ~57 nm poly-Si layers before (a-Si) and after (poly-Si) the high temperature anneal. As is clearly visible, the area below the peak corresponding to the sample exposed to 950°C is significantly smaller compared to all other peaks. Within the picture of a disrupted oxide this is explained by a redistribution of the oxygen atoms over a larger region in direction of the depth profile measurement axis, for example by the above mentioned balling-up of the interfacial oxide [15,16]. This redistribution eventually broadens the measured peak and due to the limited GD-OES resolution, parts of this broadened peak fall below the detection limit and consequently the area under the measured peak reduces.

As a rough estimation of the disrupted fraction, the oxygen signal is integrated for the crystalized samples ($I_{poly\text{-}Si}$) and the as-deposited samples ($I_{a\text{-}Si}$) in the range of the thermal oxide (grey region in Fig. 6a). The disrupted fraction was calculated according to $(I_{a\text{-}Si} - I_{poly\text{-}Si})/I_{a\text{-}Si}$.

This quantity is shown in Fig. 6b as a function of the poly-Si layer thickness and the temperature. Therein, data points not compatible with zero disrupted fraction within the uncertainty range are marked as open symbols, with the exception of the 57 nm sample annealed at 920°C, whose uncertainty range is comparably close to zero. Interestingly, these four data points correspond to the same samples that showed high recombination (Fig. 2), strong boron in-diffusion (Fig. 3) and no TMAH etch stop (Fig. 5).

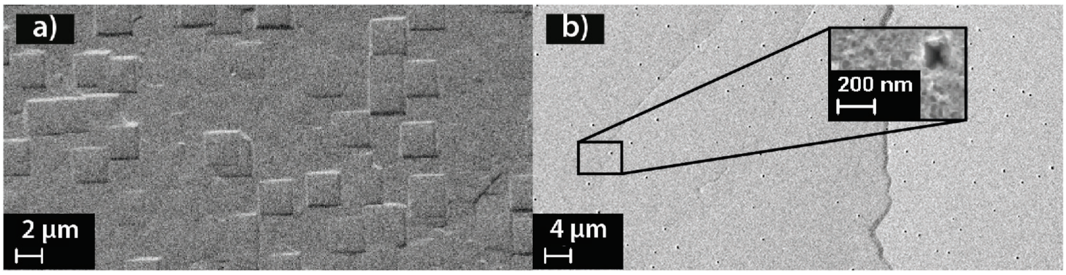

Fig. 5. Representative SEM images with a) large scale inverted pyramids as typical for global TMAH c-Si base etching and b) locally magnified pinholes by TMAH under-etching of the interfacial oxide.

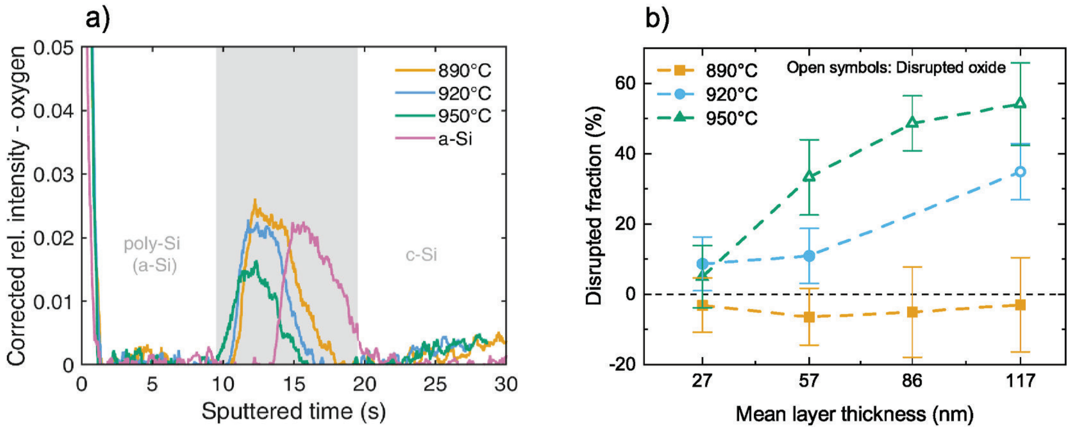

Fig. 6. a) GD-OES measured oxygen depth profiles as a function of the sputter time, exemplarily for the layers with 57 nm thickness. The signals <5 s are analysis artifacts from a correction of atmospheric contamination in the oxygen signal [31], while the peaks in the grey region originate from the interfacial oxide. b) Disrupted fraction of the interfacial oxide as a function of the poly-Si layer thickness and annealing temperature.

To summarize the just discussed findings, it is concluded that at higher annealing temperatures the interfacial oxide is disrupted for thicker layers, which is validated by (i) the increase of the recombination in the poly-Si/SiO_x structure (Fig. 2), (ii) the disproportionately strong boron in-diffusions (Fig. 3), (iii) the missing TMAH etch stop during pinhole magnification (Fig. 5) as well as (iv) the reduced oxygen signal measured by GD-OES (Fig. 6).

In a recent study by Padhamnath et al. [18] ECV profiles of (p) poly-Si/SiO_x contacts were published, which show strong in-diffusion similar to the ones presented in Fig. 3c. Therein, the interfacial oxide completely lost its diffusion barrier function for drive-in temperatures >950°C during BBr_3 ex-situ doping of initially intrinsic (i) poly-Si. In light of the strong experimental evidence of a dopant mediated oxide disruption described above and the similarity of the ECV profiles, it seems plausible that also the interfacial oxides in Ref. [18] were disrupted in a similar way.

3.3. Explanations for the interfacial oxide disruption

In the following, possible explanations for the oxide disruption are discussed. One explanation could be temperature-induced interfacial oxide disruption, which is well-known [15,16]. However, as for ~27 nm all interfacial oxides were intact even after annealing at 920/950°C, temperature alone does not fully explain the presented observations. Interestingly, for intrinsic (i) poly-Si reference layers without boron, all TMAH etch processes stopped at the interfacial oxide including also the thicker layers annealed at 920/950°C, hence the interfacial oxides were intact. Also corresponding PCD measurements of the (i) poly-Si reference layers after hydrogenation did not show a similar abrupt trend with layer thickness as observed for the doped ones (Fig. 2). Both results from the analysis of the (i) poly-Si reference samples strongly suggest that the interfacial oxide disruption is rather mediated by the temperature-dependent boron penetration than by the temperature itself. This notion is supported by the simulated thickness-dependent boron profiles discussed above (Fig. 4), where thicker layers led to stronger boron penetration, which possibly triggers the oxide disruption. A corresponding microscopic mechanism was not yet identified and will be subject of future investigation. Nevertheless, possible candidates based on literature review are briefly discussed in the following.

A dopant mediated oxide disruption was previously reported in Ref. [10], where for identical process conditions except for the initial arsenic concentration in the poly-Si, the interfacial oxide remained intact in presence of the lower concentration, while in presence of the higher concentration the oxide was totally disrupted. Unfortunately, the authors in Ref. [10] did not identify an underlying microscopic mechanism.

One objection could be, that the observed thickness dependence is not generally related to boron penetration of the interfacial oxide but rather to the magnetron sputter deposition causing a sputter damage in the interfacial oxide, which is stronger for thicker layers due to the longer deposition duration. Such passivation degrading sputter damage is well-known from transparent conductive oxide deposition in silicon heterojunction solar cells [32,33]. In the context of poly-Si/SiO_x contacts a similar effect was observed immediately after (i) a-Si deposition, but was efficiently compensated by the subsequent $POCl_3$ diffusion and hydrogenation [34]. The results in the present study differ since the samples were in-situ doped by co-sputtering of boron and the high recombination was not compensated by hydrogenation. Furthermore, the effect of an oxide disruption for the same poly-Si thickness occurring only above a threshold temperature, is not inherently explained by such a sputter damage.

Another explanation also related to the sputter deposition could be an undesired impurity in the boron sputter target, which came with a purity of only 3 N with iron being the main contaminant (180 ppm). It is consequently expected that iron is also present in the deposited a-Si layer, even though highly diluted due to silicon and boron co-sputtering. A rough estimate is provided based on the ECV-measured boron concentration and assuming equal incorporation rates of sputtered boron and iron in the layer. The iron concentration in the layers is then roughly estimated to $5{\cdot}10^{16}$ cm ^{3}. Since low recombination current densities slightly above 10 fA/cm^2 were achieved, it can be concluded, that this contamination is not an issue in general. In the context of microelectronics, the effect of iron-induced oxide breakdown is known to reduce the breakdown voltage of gate oxides, but was not linked to a physical oxide disruption [35]. Even though Fe^{3+} may replace Si^{4+} in SiO_2, a possible role of iron contamination being involved in the oxide disruption remains unclear.

The last possible explanation discussed at this point is mechanical stress in the poly-Si layer induced by crystallization. In Refs. [36,37] it was found, that for intrinsic and phosphorus doped a-Si layers the stress after crystallization was lower towards larger annealing temperatures in the range of 630 – 900°C. Assuming that this trend also holds for boron doping and can be extrapolated up to 950°C, it points in the wrong direction with respect to a stress-induced oxide disruption. It is therefore assumed that stress plays a minor role in this context, although this cannot be ruled out.

3.4. Relation of the oxide disruption to the surface recombination velocity

Even though the detailed mechanism behind the oxide disruption remains unclear, one can gain further information regarding the degradation of passivation for strong in-diffusion by taking into account not only the simulated, but also the experimentally determined boron interface concentration. Depth profiles of the in-diffused shallow boron tail were measured by ECV after TMAH etch stop at the interfacial oxide. In order to gain pseudo experimental values for the interface boron concentration $n_{B,int,exp}$, the ECV profiles were fitted by Gaussian functions with a fixed maximum position at 0 nm allowing to extrapolate the depth profile to the interface,[3] which is shown in Fig. 7a. Due to the missing TMAH etch stop, no such profiles could be measured for the samples with disrupted interfacial oxide.

The now obtained interface boron concentration $n_{B,int,exp}$ was used to determine the interface recombination velocity S_{ox}. To do so, the approach suggested by Peibst et al. [14] was used, in which an adjusted Fischer model for point contact solar cells [38] is applied to pinhole dominated carrier transport in a poly-Si/SiO_x structure. All model input parameters and corresponding determination methods are summarized in Table 2. The in-diffused shallow dopant tail was approximated by a box profile with the fitted boron interface concentration $n_{B,int,exp}$ as height. This constant concentration ensures a homogeneous resistivity $\rho(n_{B,int,exp})$ within the shallow dopant tail, enabling to deduce the emitter depth W_{emi} from the ECV determined sheet resistance R_{sheet} using $W_{emi} = \rho(n_{B,int,exp})/R_{sheet}$. As ECV measurements after TMAH etching were not possible on the samples with disrupted oxide, S_{ox} determination was only possible on the samples with intact oxide.

The parameter S_{ox} can be interpreted as representing the actual recombination velocity at the interface opposed to the experimentally accessible effective recombination velocity S_{eff}. Based on this interpretation, S_{ox} should provide information about a possible boron induced damage to the interfacial oxide in terms of an increased interface defect density, which in turn might be linked to a pre-stage of the oxide disruption.

Fig. 7b shows this interface recombination velocity S_{ox} as a function of the ECV determined boron interface concentration $n_{B,int,exp}$ whereby an exponential increase in S_{ox} towards larger $n_{B,int,exp}$ is observed. This relation is especially interesting in light of the question raised in the introduction, why the passivation of poly-Si/SiO_x contacts degrades towards stronger boron in-diffusion. Since Auger recombination can be excluded, the interface boron concentration could be a candidate for an explanation of this degradation, even though at this point no mechanism is given which would allow for a causal relation. In addition to similar ECV profiles as discussed above, Padhamnath et al. also found such an increasing relation of stronger recombination towards higher boron interface concentration [18]. Assuming that their CVD-deposited (p) poly-Si layers are basically iron-free, the similar results suggest that the penetration-mediated interfacial oxide degradation occurs also in the absence of iron.

Relations between the boron surface concentration of homogeneously doped or diffused c-Si bases and the surface recombination velocity have been studied before numerically [40] and experimentally [41]. The former study found rather linear increases in surface recombination velocity with boron surface concentration, while the latter study concludes no correlation at all between both quantities for the case of Al_2O_3 passivation. These conclusions do not fit properly to the rather exponential increase observed in Fig. 7b (note the logarithmic scale). However, in both studies the chemical surface passivation layer was deposited after the boron diffusion, which is fundamentally different for poly-Si/SiO_x contacts. Therein, the interfacial oxide as chemical passivation layer is penetrated by the boron thereby possibly inducing recombination active defects at the interface, which eventually cause the exponential increase. In this sense, rather the dopant penetration than the actual interface concentration is responsible for the passivation degradation in poly-Si/SiO_x contacts.

In summary, the exponential relation $S_{ox}(n_{B,int,exp})$ supports the idea, that towards stronger boron in-diffusion the interfacial oxide degrades as the surface recombination velocity increases and, in the extreme case, the oxide is eventually disrupted. However, a causal relation cannot be verified as the iron contamination in the boron sputter target or stress in the poly-Si layer could also be involved. Nevertheless, both cases, dopant or contamination-induced degradation and disruption of the interfacial oxide, are highly relevant for future device optimization on industrial scale where compromises between costs and purity are common.

4. Conclusion and outlook

It was observed that for higher temperatures during crystallization and also for thicker poly-Si layers the recombination increased up to a total loss of passivation due to a physical oxide disruption, a hypothesis supported by disproportionately strong boron in-diffusions, the missing TMAH etch stop as well as a reduced GD-OES oxygen signal. Interestingly, the last two effects were not observed on intrinsic reference samples, which strongly suggests a boron penetration induced degradation of the interfacial oxide. Applying the model in Ref. [14] and fitting the in-diffused ECV measured boron profiles revealed an exponential dependency of the actual surface recombination velocity on the boron concentration at the interface between interfacial oxide and c-Si base. In comparison to previous studies it is concluded that in the context of poly-Si/SiO_x contacts rather the penetration of the interfacial oxide than the actual boron interface concentration is responsible for the passivation degradation.

CRediT authorship contribution statement

Jonathan Linke: Writing – review & editing, Writing – original draft, Methodology, Investigation, Formal analysis, Conceptualization. **Raphael Glatthaar:** Writing – review & editing, Writing – original draft, Methodology, Investigation, Formal analysis, Conceptualization. **Frank**

[3] In order to avoid changes in terminology, the term „interface" refers to the interface between interfacial oxide and c-Si base originally buried below the poly-Si, which is technically the "surface" of the sample after TMAH poly-Si etch.

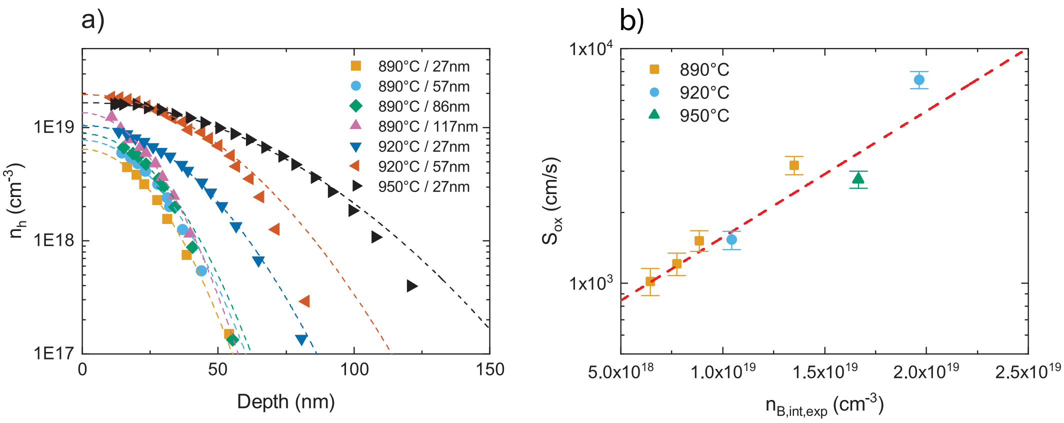

Fig. 7. a) ECV depth profiles of the active boron concentration in the c-Si base after TMAH etch and corresponding Gaussian fits indicated as dashed lines. b) Recombination velocity at the SiO_x/c-Si interface as determined by the model in Ref. [14] as a function of the interface boron concentration deduced from the fits in a). The dashed line is a guide to the eye.

Table 2
Input parameters for the model in Ref. [14], corresponding determination method, parameter value range and assumed uncertainty.

Parameter	Determination	Value range	Uncertainty
Shallow dopant tail sheet resistance	ECV	896–4950 Ω/sq	10%
Shallow dopant tail box profile height	ECV Gauss fit	6.4–20·10^{18} cm^{-3}	2 - 35·10^{16} cm^{-3}
Pinhole radius	Model in [16]	5.5–7.5 nm	1 nm
Pinhole areal density	SEM (EPD)	6.4–9.6·10^{6} cm^{-2}	1–7 ·10^{5} cm^{-2}
Recombination current density	PCD	11–25 fA/cm^2	8% [25]
Auger recombination in shallow dopant tail	ECV/EDNA	0.1–1.1 fA/cm^2	10%
Electron density in shallow dopant tail n_0	[39]	47.0–92.5 cm^{-3}	0.1–0.9 cm^{-3}

Huster: Writing – review & editing, Validation, Formal analysis. **Tobias Okker:** Investigation. **Sören Möller:** Investigation. **Giso Hahn:** Writing – review & editing, Supervision, Resources. **Barbara Terheiden:** Writing – review & editing, Supervision, Resources, Project administration, Funding acquisition.

Declaration of competing interest

The authors declare that they have no known competing financial interests or personal relationships that could have appeared to influence the work reported in this paper.

Data availability

Data will be made available on request.

Acknowledgements

The authors like to thank Uwe Breuer for conducting the SIMS measurements at Forschungszentrum Jülich GmbH. Part of this work was financially supported by the German Federal Ministry of economic affairs and climate action (FKZ0324198A, TuKaN).

References

[1] J. Schmidt, R. Peibst, R. Brendel, Surface passivation of crystalline silicon solar cells: present and future, Sol. Energy Mater. Sol. Cells 187 (2018) 39–54, https://doi.org/10.1016/j.solmat.2018.06.047.

[2] T.G. Allen, J. Bullock, X. Yang, A. Javey, S. De Wolf, Passivating contacts for crystalline silicon solar cells, Nat. Energy 4 (11) (Nov. 2019) 914–928, https://doi.org/10.1038/s41560-019-0463-6.

[3] M. Hermle, F. Feldmann, M. Bivour, J.C. Goldschmidt, S.W. Glunz, Passivating contacts and tandem concepts: approaches for the highest silicon-based solar cell efficiencies, Appl. Phys. Rev. 7 (2) (Jun. 2020), 021305, https://doi.org/10.1063/1.5139202.

[4] D. Yan, et al., Polysilicon passivated junctions: the next technology for silicon solar cells? Joule 5 (4) (Apr. 2021) 811–828, https://doi.org/10.1016/j.joule.2021.02.013.

[5] F. Feldmann, C. Reichel, R. Müller, M. Hermle, The application of poly-Si/SiOx contacts as passivated top/rear contacts in Si solar cells, Sol. Energy Mater. Sol. Cells 159 (Jan. 2017) 265–271, https://doi.org/10.1016/j.solmat.2016.09.015.

[6] B. Nemeth, et al., Polycrystalline silicon passivated tunneling contacts for high efficiency silicon solar cells, J. Mater. Res. 31 (6) (Mar. 2016) 671–681, https://doi.org/10.1557/jmr.2016.77.

[7] I.R.C. Post, P. Ashburn, G.R. Wolstenholme, Polysilicon emitters for bipolar transistors: a review and re-evaluation of theory and experiment, IEEE Trans. Electron. Dev. 39 (7) (Jul. 1992) 1717–1731, https://doi.org/10.1109/16.141239.

[8] F. Feldmann, J. Schön, J. Niess, W. Lerch, M. Hermle, Studying dopant diffusion from poly-Si passivating contacts, Sol. Energy Mater. Sol. Cells 200 (Sep. 2019), 109978, https://doi.org/10.1016/j.solmat.2019.109978.

[9] U. Römer, et al., Ion implantation for poly-Si passivated back-junction back-contacted solar cells, IEEE J. Photovoltaics 5 (2) (Mar. 2015) 507–514, https://doi.org/10.1109/JPHOTOV.2014.2382975.

[10] G.L. Patton, J.C. Bravman, J.D. Plummer, Physics, technology, and modeling of polysilicon emitter contacts for VLSI bipolar transistors, IEEE Trans. Electron. Dev. 33 (11) (Nov. 1986) 1754–1768, https://doi.org/10.1109/T-ED.1986.22738.

[11] T. Aoyama, H. Tashiro, K. Suzuki, Diffusion of boron, phosphorus, arsenic, and antimony in thermally grown silicon dioxide, J. Electrochem. Soc. 146 (5) (May 1999) 1879–1883, https://doi.org/10.1149/1.1391859.

[12] F. Feldmann, M. Bivour, C. Reichel, M. Hermle, S.W. Glunz, Passivated rear contacts for high-efficiency n-type Si solar cells providing high interface passivation quality and excellent transport characteristics, Sol. Energy Mater. Sol. Cells 120 (Jan. 2014) 270–274, https://doi.org/10.1016/j.solmat.2013.09.017.

[13] T. Yamamoto, K. Uwasawa, T. Mogami, Bias temperature instability in scaled p polysilicon gate p-MOSFET's, IEEE Trans. Electron. Dev. 46 (5) (1999) 6, https://doi.org/10.1109/16.760398.

[14] R. Peibst, et al., Working principle of carrier selective poly-Si/c-Si junctions: is tunnelling the whole story? Sol. Energy Mater. Sol. Cells 158 (Dec. 2016) 60–67, https://doi.org/10.1016/j.solmat.2016.05.045.

[15] G.R. Wolstenholme, N. Jorgensen, P. Ashburn, G.R. Booker, An investigation of the thermal stability of the interfacial oxide in polycrystalline silicon emitter bipolar transistors by comparing device results with high-resolution electron microscopy observations, J. Appl. Phys. 61 (1) (Jan. 1987) 225–233, https://doi.org/10.1063/1.338861.

[16] S.A. Ajuria, R. Reif, Early stage evolution kinetics of the polysilicon/single-crystal silicon interfacial oxide upon annealing, J. Appl. Phys. 69 (2) (Jan. 1991) 662–667, https://doi.org/10.1063/1.347346.

[17] H. Park, et al., Role of polysilicon in poly-Si/SiO_x passivating contacts for high-efficiency silicon solar cells, RSC Adv. 9 (40) (2019) 23261–23266, https://doi.org/10.1039/C9RA03560E.

[18] P. Padhamnath, N. Nampalli, A. Khanna, B. Nagarajan, A.G. Aberle, S. Duttagupta, Progress with passivation and screen-printed metallization of boron-doped monoPoly^{TM} layers, Sol. Energy 231 (Jan. 2022) 8–26, https://doi.org/10.1016/j.solener.2021.11.015.

[19] A. Morisset, et al., Conductivity and surface passivation properties of boron-doped poly-silicon passivated contacts for c-Si solar cells, Phys. Status Solidi A 216 (10) (May 2019), 1800603, https://doi.org/10.1002/pssa.201800603.

[20] J. Linke, et al., Influence of the carbon concentration on (p) poly-SiC_x layer properties with focus on parasitic absorption in front side poly-SiC_x/SiO_x passivating contacts of solar cells, IEEE J. Photovoltaics 10 (6) (2020) 1624–1631, Nov, https://doi.org/10.1109/JPHOTOV.2020.3023506.
[21] J. Steffens, Dependencies between Poly-Si Composition and Solar Cell Performance of Poly-Si/SiOx Passivating Contacts, Dissertation, University of Konstanz, Konstanz, 2020 [Online]. Available: http://nbn-resolving.de/urn:nbn:de:bsz:352-2-19tzla6vns71f7.
[22] D. Yan, A. Cuevas, S.P. Phang, Y. Wan, D. Macdonald, 23% efficient p-type crystalline silicon solar cells with hole-selective passivating contacts based on physical vapor deposition of doped silicon films, Appl. Phys. Lett. 113 (6) (Aug. 2018), 061603, https://doi.org/10.1063/1.5037610.
[23] D. Tetzlaff, et al., Introducing pinhole magnification by selective etching: application to poly-Si on ultra-thin silicon oxide films, Energy Proc. 124 (Sep. 2017) 435–440, https://doi.org/10.1016/j.egypro.2017.09.270.
[24] A. Kimmerle, J. Greulich, A. Wolf, Carrier-diffusion corrected J0-analysis of charge carrier lifetime measurements for increased consistency, Sol. Energy Mater. Sol. Cells 142 (Nov. 2015) 116–122, https://doi.org/10.1016/j.solmat.2015.06.043.
[25] A.L. Blum, et al., Interlaboratory study of eddy-current measurement of excess-carrier recombination lifetime, IEEE J. Photovoltaics 4 (1) (Jan. 2014) 525–531, https://doi.org/10.1109/JPHOTOV.2013.2284375.
[26] FlexPDE, PDE solutions Inc [Online]. Available: www.pdesolutions.com.
[27] K.R. McIntosh, P.P. Altermatt, A freeware 1D emitter model for silicon solar cells, in: 35th IEEE Photovoltaic Specialists Conference, Jun. 2010, https://doi.org/10.1109/PVSC.2010.5616124. Honolulu, HI, USA, 002188–002193.
[28] V.E. Borisenko, S.G. Yudin, Steady-state solubility of substitutional impurities in silicon, Phys. Status Solidi A 101 (1) (May 1987) 123–127, https://doi.org/10.1002/pssa.2211010113.
[29] K. Ryu, Y.-W. Ok, C.-J. Choi, A. Rohatgi, Study of lifetime degradation in n-type silicon due to oxidation of boron-rich layer, in: IEEE 39th Photovoltaic Specialists Conference (PVSC), Jun. 2013, pp. 2655–2658, https://doi.org/10.1109/PVSC.2013.6745019. Tampa, FL, USA.
[30] V.D. Mihailetchi, H. Chu, J. Lossen, R. Kopecek, Surface passivation of boron-diffused junctions by a borosilicate glass and in situ grown silicon dioxide interface layer, IEEE J. Photovoltaics 8 (2) (Mar. 2018) 435–440, https://doi.org/10.1109/JPHOTOV.2018.2792422.
[31] J. Steffens, G. Hahn, B. Terheiden, Towards a fast determination of the hydrogen concentration in thin passivating a-Si:H layers using GD-OES, AIP Conf. Proc. 1999 (2018), 020021, https://doi.org/10.1063/1.5049260.
[32] L. Tutsch, M. Bivour, W. Wolke, M. Hermle, J. Rentsch, Influence of the transparent electrode sputtering process on the interface passivation quality of silicon heterojunction solar cells, in: 33rd European PV Solar Energy Conference and Exhibition (EUPVSEC), 2017, https://doi.org/10.4229/EUPVSEC20172017-2AV.3.8. Amsterdam, The Netherlands.
[33] B.-M. Meiners, D. Borchert, S. Hohage, S. Holinksi, P. Schäfer, Degradation of hydrogenated amorphous silicon passivation films caused by sputtering deposition, Phys. Status Solidi A 212 (8) (Aug. 2015) 1817–1822, https://doi.org/10.1002/pssa.201431923.
[34] J. Steffens, J. Rinder, G. Hahn, B. Terheiden, Compensation of the sputter damage during a-Si deposition for poly-Si/SiOx passivating contacts by ex-situ P-doping, AIP Conf. Proc. 2147 (2019), 040018, https://doi.org/10.1063/1.5123845.
[35] W.B. Henley, L. Jastrzebski, N.F. Haddad, Effects of iron contamination in silicon on thin oxide breakdown and reliability characteristics, J. Non-Cryst. Solids 187 (Jul. 1995) 134–139, https://doi.org/10.1016/0022-3093(95)00125-5.
[36] H. Miura, H. Ohta, N. Okamoto, T. Kaga, Crystallization-induced stress in silicon thin films, Appl. Phys. Lett. 60 (22) (Jun. 1992) 2746–2748, https://doi.org/10.1063/1.106864.
[37] H. Miura, N. Okamoto, Crystallization-induced stress in phosphorus-doped amorphous silicon thin films, J. Appl. Phys. 75 (9) (1994) 4747–4749, https://doi.org/10.1063/1.355932.
[38] H. Plagwitz, R. Brendel, Analytical model for the diode saturation current of point-contacted solar cells, Prog. Photovoltaics Res. Appl. 14 (1) (Jan. 2006) 1–12, https://doi.org/10.1002/pip.637.
[39] Dopant ionisation calculator with default settings, PV Lighthouse (Nov. 08, 2021). https://www.pvlighthouse.com.au.
[40] P.P. Altermatt, Models for numerical device simulations of crystalline silicon solar cells—a review, J. Comput. Electron. 10 (3) (Sep. 2011) 314–330, https://doi.org/10.1007/s10825-011-0367-6.
[41] L.E. Black, T. Allen, K.R. McIntosh, A. Cuevas, Effect of boron concentration on recombination at the p-Si-Al_2O_3 interface, J. Appl. Phys. 115 (9) (Mar. 2014), 093707, https://doi.org/10.1063/1.4867643.